

Gas flow in Callovo-Oxfordian claystone (COx): results from laboratory and field-scale measurements

J. F. HARRINGTON^{1*}, R. DE LA VAISSIÈRE², D. J. NOY¹, R. J. CUSS¹ AND J. TALANDIER²

¹ British Geological Survey, Keyworth, Nottingham NG12 5GG, UK

² Agence Nationale pour la Gestion des Déchets Radioactifs (ANDRA), Chatenay-Malabry, France

[Received 19 December 2011; Accepted 19 November 2012; Associate Editor: Nicholas Evans]

ABSTRACT

To understand the fate and impact of gas produced within a repository for radioactive waste, a series of laboratory and field scale experiments have been performed on the Callovo-Oxfordian claystone (COx), the proposed host rock for the French repository. Results show the movement of gas is through a localized network of pathways, whose properties vary temporarily and spatially within the claystone. Significant evidence exists from detailed laboratory studies for the movement of gas along highly unstable pathways, whose aperture and geometry vary as a function of local stress, gas and porewater pressures. The coupling of these parameters results in the development of significant time-dependent effects, impacting on all aspects of COx behaviour, from gas breakthrough time, to the control of deformation processes. Variations in gas entry, breakthrough and steady-state pressures are indicative of microstructural heterogeneity which exerts an important control on the movement of gas. The localization of gas flow is also evident in preliminary results from the large scale gas injection test (PGZ) where gas flow is initially focussed within the excavation damaged zone (EDZ), which acts as a preferential pathway for gas. Numerical models based on conventional two-phase flow theory are unable to adequately describe the detailed observations from laboratory tests.

KEYWORDS: gas flow, geological disposal, modelling, radioactive waste.

Introduction

In a repository for radioactive waste, corrosion of ferrous materials under anoxic conditions, combined with the radioactive decay of the waste and the radiolysis of water, will lead to the formation of hydrogen. If the rate of gas production exceeds the rate of gas diffusion within the pores of the barrier or host rock, a discrete gas phase will form (Weetjens and Sillen, 2006; Ortiz *et al.*, 2002; Wikramaratna *et al.*, 1993). Under these conditions, gas will continue to accumulate until its pressure becomes sufficiently large for it to enter the surrounding material. In a clay-based geological disposal facility (GDF), four primary

phenomenological models describing gas flow can be defined: (1) gas movement by diffusion and/or solution within interstitial fluids along prevailing hydraulic gradients; (2) gas flow in the original porosity of the fabric, commonly referred to visco-capillary (or 2-phase) flow; (3) gas flow along localized dilatant pathways, which may or may not interact with the continuum stress field; and (4) gas fracturing of the rock similar to that performed during hydrocarbon stimulation exercises. There is now a growing body of evidence (Horseman *et al.*, 1996, 2004; Harrington and Horseman, 1999; Angeli *et al.*, 2009; Harrington *et al.*, 2009) that in the case of plastic clays and in particular bentonite, classic concepts of porous medium two-phase flow are inappropriate and continuum approaches to modelling gas flow may be questionable, depending on the scale of the processes and resolution of the numerical model.

* E-mail: jfha@bgs.ac.uk

DOI: 10.1180/minmag.2012.076.8.43

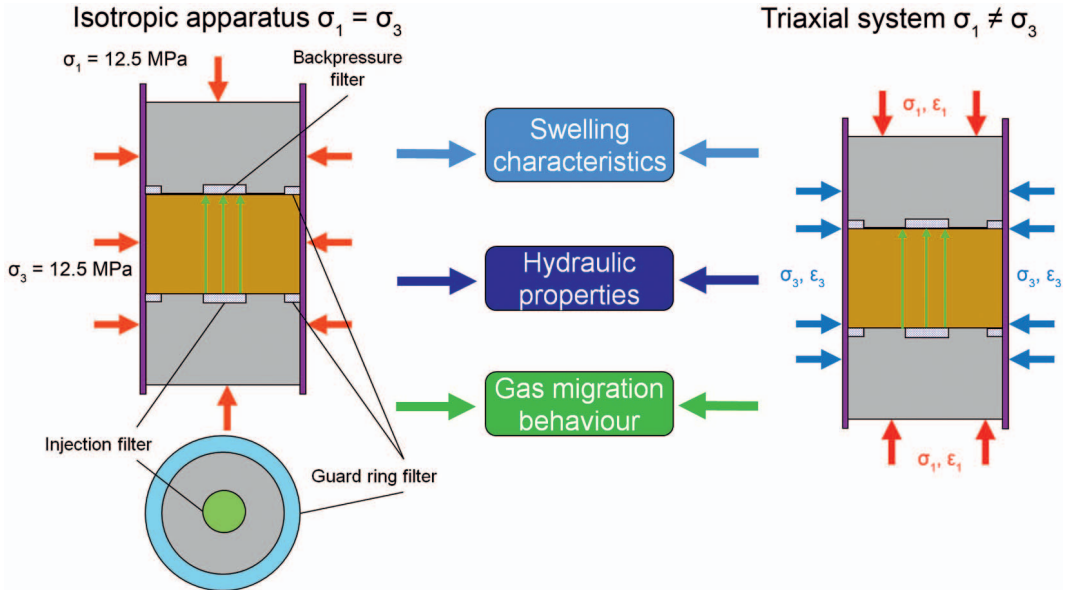


FIG. 1. Schematic showing the sample assemblies for both isotropic and triaxial test systems. Both geometries can be used to define the swelling/consolidation characteristics, hydraulic properties and the gas migration behaviour. The sample in the triaxial system is mounted horizontally. Isotropic tests were performed perpendicular to bedding whereas the triaxial test was performed on a sample cut parallel to bedding.

However, the exact mechanisms controlling gas entry, flow and pathway sealing in general clay-rich media are not fully understood and the ‘memory’ of such pathways could impair barrier performance.

To investigate these issues the British Geological Survey (BGS) has performed a series of laboratory-scale tests on preserved samples of the Callovo-Oxfordian claystone (COx), a candidate host rock for the disposal of radioactive waste material in France. In parallel, Andra have undertaken a series of field based experiments examining the potential for gas flow in the host rock and the role of the excavation damaged zone (EDZ) in the movement of gas within the potential GDF.

Laboratory study

Two experimental geometries were used in the laboratory to investigate the mechanisms and processes governing gas flow in the COx (Fig. 1). In the first system, samples were subject to an isotropic confining stress, using injection platen mounted on the base of the specimen. In the second system, axial and radial stress were controlled independently with continuous strain

monitoring (both axially and radially), providing real-time data on the volume change of the sample. Both systems consist of five main components: (1) a specimen assembly; (2) a 70 MPa rated pressure vessel and associated confining pressure system; (3) a fluid-injection system; (4) a backpressure system; and (5) a PC-based data acquisition system. A novel feature of both experimental set ups is the use of porous annular guard ring filters around the inflow and outflow filters. The pressures in these two guard rings can be independently monitored. The advantages of the guard ring approach are: (1) pore pressure evolution can be studied; (2) hydraulic anisotropy can be quantified in a single test; (3) a check can be made of flow symmetry in the specimen; (4) excess gas pressure at gas entry can be determined; and (5) uncertainties associated with possible side wall leakage can be eliminated from data interpretation. Permeants (gas and water) are injected at the base of the specimen¹ to minimize

¹ The sample in the triaxial system is mounted horizontally.

the chance of slug flow during gas testing. The hydraulic fluid used during this study was based on a synthetic porewater solution, the composition of which was provided by Andra.

Volumetric flow rates to and from the core are controlled or monitored using a pair of ISCO-260, Series D, syringe pumps operated from a single digital control unit. The position of each pump piston is determined by an optically encoded disc graduated in segments equivalent to a change in volume of 16.6 nl. Movement of the pump piston is controlled by a micro-processor which continuously monitors and adjusts the rate of rotation of the encoded disc using a DC-motor connected to the piston assembly via a geared worm drive. This allows each pump to operate in either constant pressure or constant flow modes. A programme written in *LabVIEW* records data from the pump at pre-set time intervals. Testing is performed in an air-conditioned laboratory at a nominal temperature of 20°C with a minor diurnal variation of typically $\pm 0.25^\circ\text{C}$.

Test material

Upon receipt of the preserved T1-cell core barrels at BGS, the material was catalogued and stored under refrigerated conditions of 4°C to minimize biological and chemical degradation. Test specimens were manufactured by a combination of dry core-drilling (with gas flushing and vacuum removal of fines), diamond slicing and surface grinding, or produced by machine lathing, a more sympathetic process which is less likely to induce damage within the material as a result of sample preparation. All specimens were accurately measured using a digital micrometer and

weighed prior to installation within the apparatus, to provide an estimate of the pre-test geotechnical properties (Table 1). The minor differences in geotechnical properties between specimens COx-1 and -2 (which come from neighbouring sections of the same core barrel) are illustrative of the localized heterogeneity within the Callovo-Oxfordian formation, the importance of which may be significant during gas and water testing.

Data reduction and modelling approaches

Variable moving average smoothing was applied to all flow data to remove background experimental noise associated with pump switching and minor diurnal variations in temperature.

Hydraulic flow

An equation describing porewater flow can be obtained by combining Darcy's Law with the equation of fluid mass conservation to give (de Marsily, 1986):

$$\frac{S_s}{\rho_w g} \frac{\partial p_w}{\partial t} = \nabla \cdot \left(\frac{k_i}{\mu_w} (\nabla p_w + \rho_w g \nabla z) \right) + Q \quad (1)$$

where S_s is the specific storage (m^{-1}), k_i is the intrinsic permeability (m^2), ρ_w is the density of water (kg m^{-3}), g is the acceleration due to gravity (m s^{-2}), μ_w is the viscosity of water (Pa s), p_w is the pore-water pressure (Pa), z is the vertical coordinate (m) and Q is the rate of fluid volume injection per unit volume of porous medium (s^{-1}). This equation is solved here by the finite element method for an axisymmetric two dimensional domain subject to specified head and specified

TABLE 1. Provisional basic physical properties of the three test specimens. An assumed specific gravity for the mineral phases of 2700 kg m^{-3} (Zhang *et al.*, 2007) was used in these calculations. Measurements for sample COx-2 are provisional as the test remains on-going.

Specimen	Core barrel	Length (mm)	Diameter (mm)	Moisture content (%)	Dry density (kg m^{-3})	Porosity (%)	Saturation (%)	
COx-1	Pre-test	EST27367	53.9	54.4	6.1	2310	14.6	97
	Post-test		54.1	54.5	6.7	2290	15.2	100
COx-2	Pre-test	EST27367	55.0	54.4	6.6	2260	16.5	91
	Post-test		82.5	55.9	6.2	2310	14.8	96
SPP-2	Pre-test	EST30341	82.5	55.9	7.0	2290	15.5	100
	Post-test		82.6	55.9	7.0	2290	15.5	100
Zhang <i>et al.</i> (2007)	—	—	—	7.7	2250	16.8	—	

flow boundary conditions. Hydraulic head, h (m), is related to the pore-water pressure by the equation $p_w = \rho_w g(h - z)$.

In order to model the consolidation data, it is necessary to couple the porewater flow equation to equations for the stress-strain relationships. The porewater equation for this takes the form (Huyakorn and Pinder, 1983):

$$\nabla \cdot \left(\frac{k_i}{\mu_w} (\nabla p_w + \rho_w g \nabla z) \right) = \phi \beta \frac{\partial p_w}{\partial t} + \frac{\partial}{\partial t} (\nabla \cdot \mathbf{u}) \tag{2}$$

where ϕ is the porosity, β is the fluid compressibility (Pa^{-1}), and \mathbf{u} is the vector of solid phase displacements (m). For the case of elastic plane strain, the equations for the displacements are:

$$\frac{E}{2(1+\nu)} \nabla^2 \mathbf{u} + \frac{E}{2(1+\nu)(1-2\nu)} \nabla (\nabla \cdot \mathbf{u}) - \nabla p_w = 0 \tag{3}$$

in which E is Young's modulus (Pa) and ν is Poisson's ratio. Equations 2 and 3 are solved using the finite element code *STAFAN* (Intera, 1983). The Young's modulus, E , and Poisson's ratio, ν , can be related to the solid phase compressibility, α , and the specific storage, S_s , by the equations (de Marsily, 1986):

$$\alpha = \frac{3(1-2\nu)}{E} \tag{4}$$

and

$$S_s = \rho g (\alpha + \phi \beta) \tag{5}$$

where ρ is the porewater density, g the acceleration due to gravity, ϕ the porosity and β the compressibility of the porewater.

Gas flow

The equation for steady-state flow of gas as a single phase in a porous medium may be written by combining the mass continuity equation with a generalization of Darcy's law as follows:

$$\nabla \cdot \left(\frac{\rho_g k_g}{\mu_g} \nabla (p_g) \right) = 0 \tag{6}$$

where p_g is the gas pressure (Pa), ρ_g is the gas density (kg m^{-3}), $k_g = k_{rg}$, k_i is the effective gas

permeability (m^2), and μ_g is the gas viscosity (Pa s). Assuming ideal gas behaviour and a constant value for k_g , equation 6 can be integrated along a 1D flow path to obtain an expression for the flow rate at STP, Q_{st} , in terms of the pressures at either end of the path:

$$Q_{st} = \frac{v_{mst} k_g A}{2RT \mu_g L} (p_{gi}^2 - p_{go}^2) \tag{7}$$

where v_{mst} is the molar volume of the gas at STP, A is the specimen's cross-sectional area, L is the specimen length, R is the gas constant, T is the absolute temperature, p_{gi} is the gas pressure at injection, and p_{go} the pressure at outlet. Although gas pressure p_{go} cannot be measured directly in these experiments, it can be related to the backpressure of the water at the downstream end of the specimen, p_{wo} , by the relationship $p_{go} = p_{wo} + p_{co}$, where p_{co} is the apparent capillary threshold pressure.

Consolidation response

In tests COx-1 and -2 the confining stress was applied in a number of steps to elicit the elastic moduli of each sample. Based on the total volume of fluid expelled, analysis of the consolidation data yields reasonably high values for the drained bulk modulus, ranging from 1490 to 2262 MPa (Table 2). These values reflect the indurated nature of the material and suggest little, if any, damage has occurred between field sampling and laboratory testing. Commensurate values for Young's modulus were found to range from 1764 to 2629 MPa which are a little lower than those reported in Andra (2005). Finite element coupled deformation and porewater flow modelling of the consolidation data yielded axial permeabilities ranging from 2.2 to $4.0 \times 10^{-21} \text{ m}^2$, with radial permeability in the range 6.3 to 10×10^{-21} . It should be noted that as confining stress increased, axial and radial permeability both decreased slightly. Estimates for specific storage (based on the values of Young's modulus and Poisson's ratio obtained in the finite element modelling and using equations 4 and 5) were found to vary from $7.2 \times 10^{-6} \text{ m}^{-1}$ to $8.9 \times 10^{-6} \text{ m}^{-1}$ (7.3 to $9.1 \times 10^{-10} \text{ Pa}^{-1}$).

Hydraulic properties

During hydraulic testing the confining and back-pressure applied to each sample were maintained

TABLE 2. Provisional consolidation data for test specimens COx-1 and -2 during test stages [2] and [3]. The start value for void ratio [1] is based on the pre-test measurement. Values for Young's modulus are based on a Poisson's ratio of 0.3 (Wileveau and Bernier, 2008). Values in parentheses are derived from finite element modelling.

Stage no.	Average effective stress (MPa)	Void ratio (at end of stage)	Volumetric strain (%)	Drained compressibility $\beta/10^{10}$ (Pa^{-1})	Drained bulk modulus (MPa)	Young's modulus (MPa)
Data for COx-1						
1	5.0	0.175	—	—	—	—
2	6.5	0.174	0.07	4.4	2262	2629 [1370]
3	8.0	0.173	0.16	6.4	1574	1870 [1370]
Data for COx-2						
1	5.0	0.193	—	—	—	—
2	6.5	0.192	0.09	5.6	1759	2092 [1350]
3	8.0	0.191	0.19	6.7	1490	1764 [1250]

constant at 12.5 and 4.5 MPa, respectively. The pressure at the injection filter was then raised to 7.5 MPa and held constant for sufficient time to establish a steady state condition. Once complete, the injection pressure was once again reduced to 4.5 MPa ready for gas testing. During hydraulic tests, the evolution in flow at injection and backpressure filters were monitored, along with the changes in guard ring pressure. To analyse the data, a second finite element porewater flow model was created to simulate the hydraulic tests (Fig. 2). It was found that good fits to the data could be obtained by setting axial permeability between 1.6 and $2.0 \times 10^{-21} \text{ m}^2$ and radial permeability from 4.0 to $5.0 \times 10^{-21} \text{ m}^2$. Specific storage was found to range from 5.4 to 6.0×10^{-6} (5.5 to $6.1 \times 10^{-10} \text{ Pa}^{-1}$). To improve model fits for specimen COx-2, a bimodal model was developed setting radial permeability to $8.8 \times 10^{-21} \text{ m}^2$ and $22.4 \times 10^{-21} \text{ m}^2$ at the injection and backpressure ends, respectively. This corresponds to an anisotropy in the permeability of 5.5 at the injection end and 14 at the backpressure end. This improved the fit to the guard ring data with very little change to the fit for the flow data indicating the important role fine-scale heterogeneities play in determining the pressure distribution within the sample.

Gas behaviour

The gas pressure gradient across sample COx-1 was slowly increased in a stepwise manner from

6.5 to 12.0 MPa over a 600 day period (Fig. 3). A small emergent flux was noted during the early stages of testing, which was found to vary with the magnitude of the gas pressure. Although the origin of this flux remains unclear, the discharge rates are comparable to those observed during hydraulic testing, suggesting the flux may be aqueous in nature relating to slug flow caused by residual water displaced from the injection filter. A similar response was observed during the initial gas stage of test COx-2. This was clearly slug flow, as the discharge rate levelled at a zero flow condition after 60 days (Fig. 4).

By independently cross-plotting the measured outflow and the injection guard ring (IGR) pressure against gas pressure at the inlet filter, it is possible to derive an estimate for the gas entry pressure. In this way, the value was found to range between 0.9 and 1.3 MPa. These values are low and may reflect localized features within the clay. Data suggests these discrete features are discontinuous and that gas is unable to propagate across the sample as is exemplified by the fact that outflow showed no correlation to changes in IGR pressure during the first 170 days of gas testing. There is also evidence in the variation in guard ring pressures (Fig. 5) for the temporal and spatial evolution of these pathways. In stark contrast, test COx-2 (Fig. 6) exhibits a gas entry pressure in excess of 10.0 MPa. At these elevated pressures, there is evidence of gas penetration signified by the increase in IGR pressure observed at around 416 days. However, close inspection of the guard ring data suggests the clay exhibits some form of

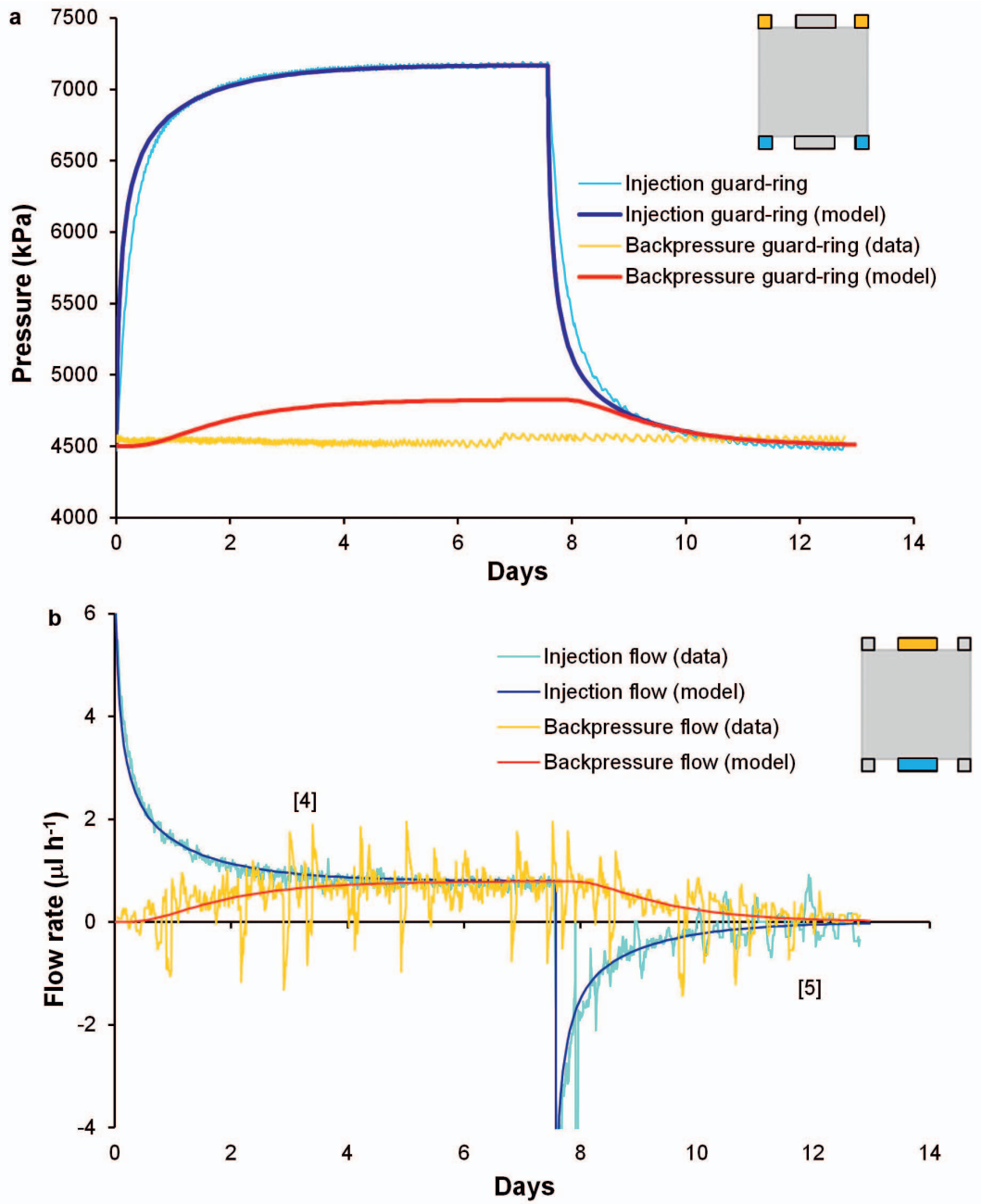


FIG. 2. Example of hydraulic response showing data and model outputs for test CO_x-1. (a) Plot showing the comparison between observed and modelled guard ring pressures; (b) a comparison of observed and predicted flow rates from the injection and back pressure filters. With the exception of the backpressure guard ring response, a good agreement between the model and data is observed.

GAS FLOW IN CALLOVO-OXFORDIAN CLAYSTONE

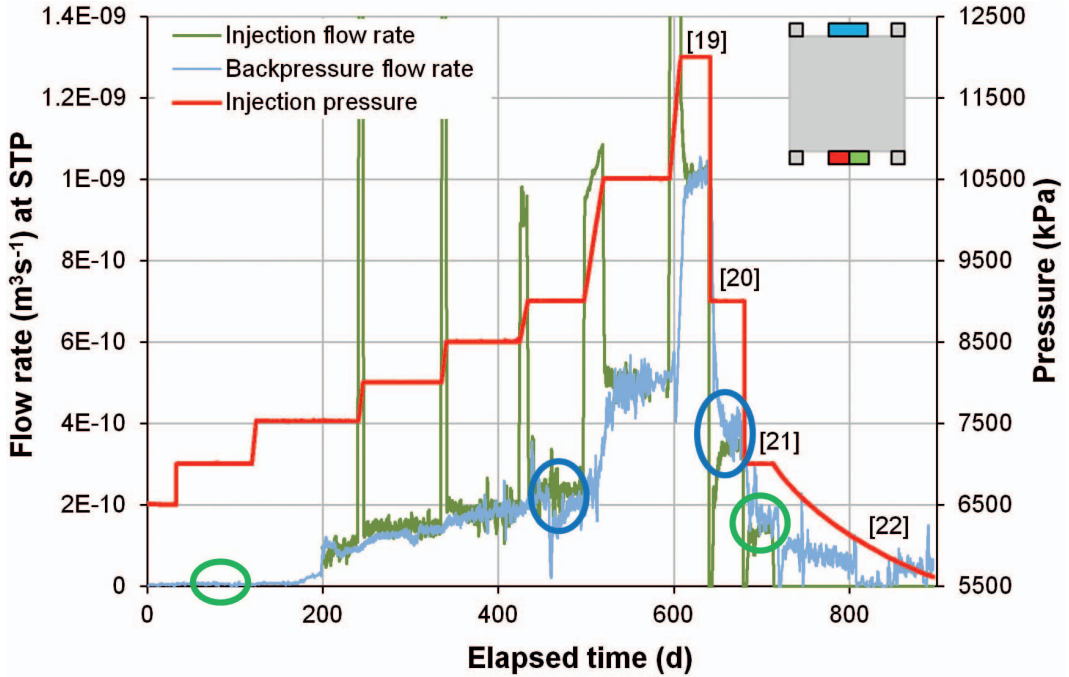


FIG. 3. Gas flow rates at the injection and backpressure filters during the gas injection test COx-1. The large spikes in injection flux relate to the compression of the gas phase during constant flow rate tests. The blue and green circles highlight hysteresis in the flow response.

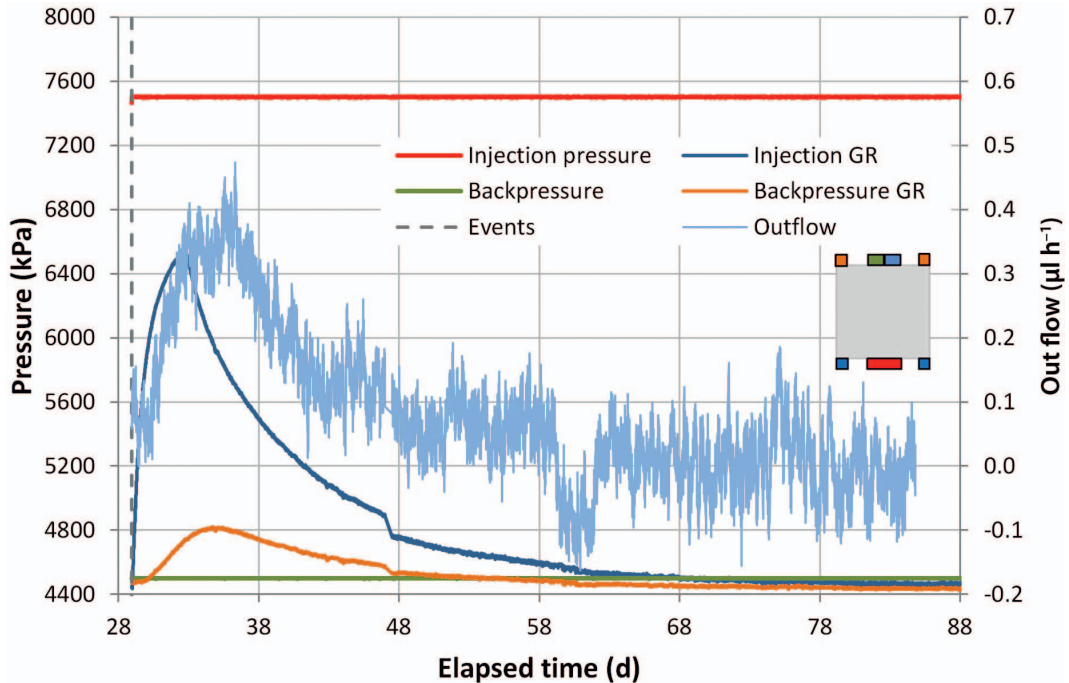


FIG. 4. Gas flow rates and guard ring pressures at the injection and backpressure filters during the initial gas injection test of COx-2. The characteristic shape of the GR and outflow response is symptomatic of hydraulic 'slug' flow.

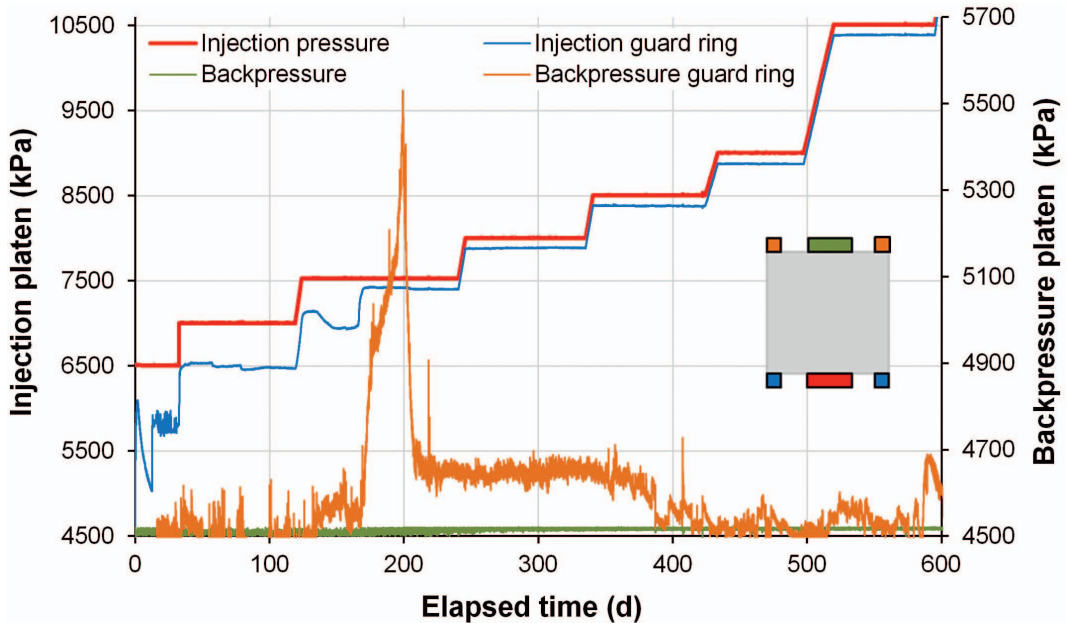


FIG. 5. Pressure data from the injection, backpressure and guard ring filters during the gas injection test COx-1. Spontaneous changes in GR pressure are indicative of highly unstable pathway flow.

spontaneous self-sealing, as thereafter IGR pressures decline, indicating a reduction in pathway permeability signifying self-sealing within the clay. While orientated parallel to bedding, sample COx-SPP-2 exhibits similarly high gas entry pressures to those of COx-2. Although these two samples come from different core barrels, it is likely their properties reflect those of ‘intact’ (or at least ‘less damaged’) COx.

Major gas breakthrough occurred in test COx-1 after 170 days of testing. This was signified by a spontaneous increase in discharge rate, ultimately leading to a quasi steady state. Analysis of flux and pressure data indicates dynamic flow behaviour and time-dependent propagation of gas pathways across the specimen, signified by spontaneous changes in flux and guard ring pressure (Figs 3 and 5). Based on these observations, the excess gas breakthrough pressure² for the claystone is estimated to be ~2 MPa for sample COx-1 and in excess of 6 MPa for samples COx-2 and SPP-1.

Additional increments in gas pressure clearly show the slow temporal evolution of gas permeability within the specimen, with flux taking around 20 days (or longer) to attain a quasi steady state (Fig. 3). This can be explained by time-dependent drainage (porous medium concepts) or pressure induced dilatancy and accompanied drainage, depending on the mechanism invoked. Spontaneous increases/decreases in both guard ring pressures and downstream flux occur throughout the test and are symptomatic of highly unstable dynamic pathways which open and close in an apparently random nature. Such observations are difficult to reconcile with standard porous medium concepts.

As gas pressure in COx-1 is reduced from day 641 onwards the asymptote of each subsequent steady state is significantly higher (for both flux and pressure) than that observed during the initial pressurization phase (Fig. 3). Hysteresis between drainage and imbibition responses is common (Zweigel *et al.*, 2006; Harrington *et al.*, 2009) and signifies a non-recoverability in the system which can result from a number of reasons, including incomplete resaturation, plastic strains around dilatant pathways and fabric alteration, though some of these effects may be recovered with the sufficient passage of time.

² Excess gas pressure is equal to the difference between the measured injection pressure and reference porewater backpressure.

GAS FLOW IN CALLOVO-OXFORDIAN CLAYSTONE

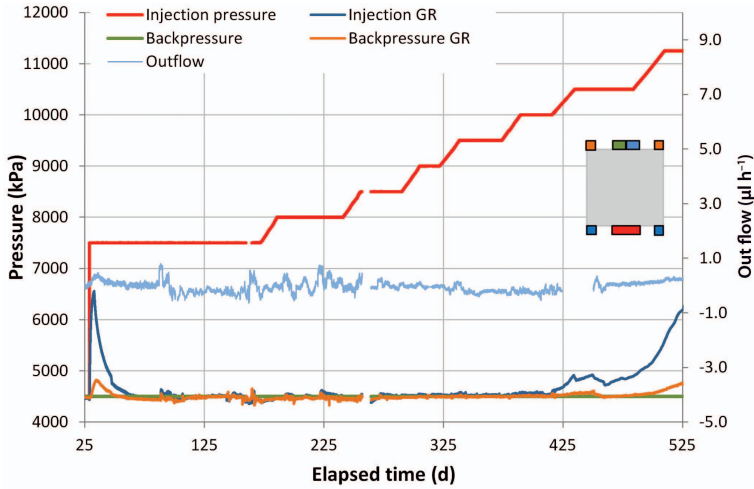


FIG. 6. Injection, backpressure and guard ring filter pressures and outflow data plotted against elapsed time in days (test COx-2). The early spike in GR pressure and the small emergent outflow are symptomatic of ‘slug’ flow. The data exhibits no obvious signs of gas flow within the clay below a gas pressure of 10.0 MPa (signified by a change in IGR pressure).

When the injection pump is switched off, gas pressure in the injection filter slowly decays and is referred to as a shut-in stage. Figure 7 shows a plot of the measured and predicted gas pressures during this time. The latter is derived from the solution to the governing differential equation for the axial flow of gas through the apparatus during a shut-in stage which is given in Harrington and Horseman (1999) as:

$$p_{gi} = p_{go} \left[\frac{(p_{gio} + p_{go}) \exp(Ht) + (p_{gio} + p_{go})}{(p_{gio} + p_{go}) \exp(Ht) - (p_{gio} + p_{go})} \right] \quad (8)$$

where p_{gio} is the gas pressure at the start of the shut-in stage and H is defined as:

$$H = \frac{2Bp_{go}}{V_{gio}} \quad (9)$$

where B is a transport variable defined as:

$$B = \frac{k_g A_s}{2\mu_g L}$$

and V_{gio} is the initial volume of gas at the start of the shut-in stage. Using this solution a fit to the data (Fig. 7) can be achieved with the following parameters: $A_s = 3.142 \times 10^{-4} \text{ m}^2$ (equates to the cross-sectional area of the central injection and backpressure filters); $k_g = 2.55 \times 10^{-21} \text{ m}^2$; $p_{co} =$

$1 \times 10^{-6} \text{ Pa}$. From these parameters we can estimate the capillary pressure to be 1.0 MPa. The analysis of the shut-in stage confirms a very low gas entry pressure for sample COx-1.

Post-test measurements of desaturation from tests COx-1 and SPP-1 indicate no discernible displacement of interstitial fluid from the original porosity (Table 1). This and the visual observations of localized degassing (Fig. 8) strongly indicate gas flow is through localized pathway dilation.

To help interpretation of the data, preliminary numerical modelling of the gas data has been undertaken using *TOUGH2* and a series of characteristic function parameters based on the van Genuchten formulation. However, attempts to model the data in its entirety, have to date, proved elusive. By alteration of the residual saturation and gas permeability functions, it is possible to fit sections of the data to the model predictions. However, this is commonly to the detriment of other experimental data. Consistent functional fits to the guard ring pressure responses have not been possible, although fits to discrete sections of the data can be achieved.

The inability of classic porous medium models to adequately represent the data is not surprising when one looks at the response from the triaxial test SPP-1 prior to and after gas breakthrough. Figure 9 clearly shows that gas flow is accompanied by a small, but well defined volume

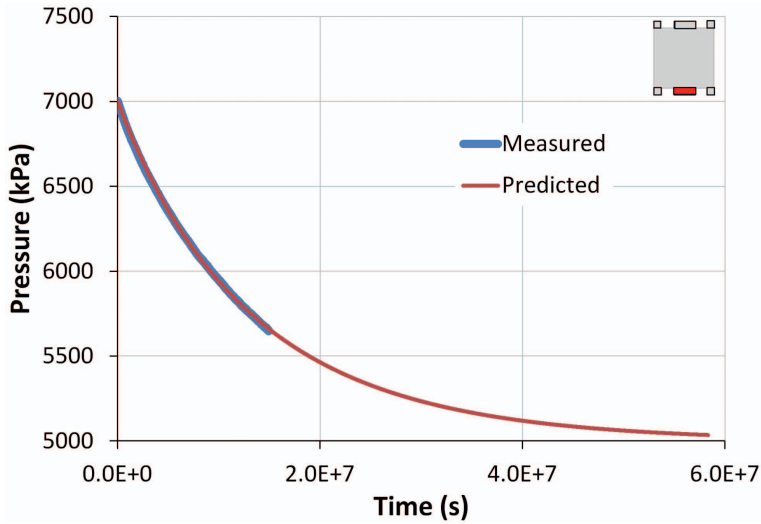


FIG. 7. Shut-in response for test COx-1. The protracted nature of the shut-in response is a function of the initial gas volume and the non-linearity in the gas flow law. However, a good numerical fit to the data is obtained allowing a prediction of the capillary threshold pressure to be made.

increase of the sample, which cannot be explained by compressibility calculations. The data clearly exhibits time dependent strain. As dilation increases so does the volumetric discharge from the sample. These data conclusively demonstrate that permeability is a dependent variable, integrally

linked to the conductive pathways aperture (in this test, manifest as volumetric strain). It is interesting to note that the observed increase in radial strain is non-uniform suggesting localized flow within the sample. This supports previous observations based on the guard ring response.



FIG. 8. Photograph showing the discharge of gas from the injection face of sample COx-1, following submersion in glycerol and gentle heating (the imprint of the central filter disc is clearly visible in the photo). The discharge of gas was both localized and often episodic, with discrete streams of gas bubbles released following a quiescent periods of inactivity.

GAS FLOW IN CALLOVO-OXFORDIAN CLAYSTONE

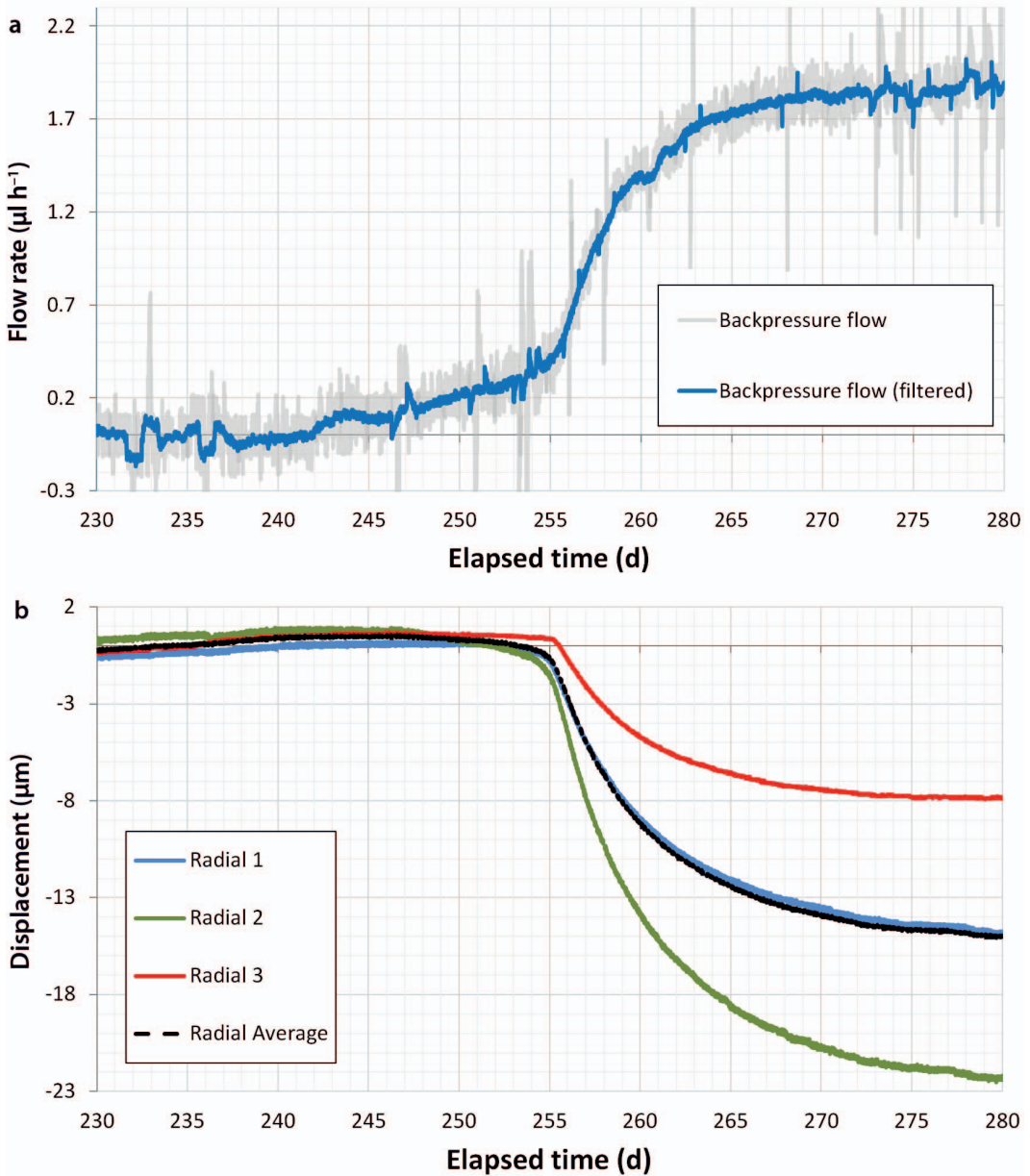


FIG. 9. Triaxial data from test SPP-1. (a) Plot showing the slow time-dependent evolution in flux out of the core; (b) showing the sample dilating in response to changes in gas outflow.

Field study

An *in situ* gas experiment in the French Underground Research Laboratory (URL) has been set-up to observe gas percolation into claystone. The experiment, PGZ1 (perturbation induced by gas), was initiated in the summer of

2009. The aim of the experiment was to undertake a gas-injection test in order to characterize the gas transfer properties in the COx formation, with the view to confirming both the parameters and limits of traditional biphasic models and to provide additional support in describing gas transfer

behaviour, such as gas entry pressure and the gas pressure above which pathway dilation occurs.

PGZ1 experimental set-up

The experimental layout consists of three boreholes (Fig. 10). The two boreholes drilled from the GED drift (PGZ1201 and PGZ1202) are equipped with a triple packer system to monitor water/gas pressure. They are 0.9 m distant from each other, parallel and inclined at 35° to the horizontal i.e. oriented parallel to the maximum stress. Borehole PGZ1031, drilled from the GEX drift, is equipped with a multiple magnetic extensometer probe for observation of the axial deformation during the gas injection stage. Borehole PGZ1031 is also inclined but at 48° to the horizontal and crosses vertically above the bottom packer of PGZ1201.

Test sequence and measurements

All hydraulic and gas injection experiments were undertaken through interval PRE02. The first test phase (HYDRO1), using synthetic water, was performed in September 2009. The HYDRO1 consisted of a pulse test followed by a constant head test. Following a recovery period to aid the

dissipation of residual porewater pressures, the synthetic fluid was carefully displaced using nitrogen gas under equilibrium conditions (i.e. porewater pressure). The second test phase (GAS1) was performed between February 2010 and April 2011 and consisted of a series of constant gas injection flow rates (GRI_x), separated by discrete recovery periods (GRIS_x) in which the gas pressure was allowed to decay. The maximum gas pressure imposed on the system was 9.1 MPa which is well below minimum principal stress of around 12.3 MPa (obtained from a fracture test in a deep borehole). The third test phase (HYDRO2) was performed in June 2011 after the gradual extraction of gas (GRE).

Figure 11 shows the measured pressure and gas flow rate from boreholes PGZ1201 and PGZ1202. The porewater pressures observed in boreholes PGZ1201 and PGZ1202 show a clear drop in interstitial pressure from October 2009 onwards. This can be simply explained by the drainage effect caused by the installation of borehole PGZ1031, which passed at a minimum distance of 1.14 m from the test interval PRE02 (de la Vaissière and Talandier, 2012).

Both hydraulic tests (HYDRO1 and HYDRO2) were interpreted using a fitting procedure with a composite radial model

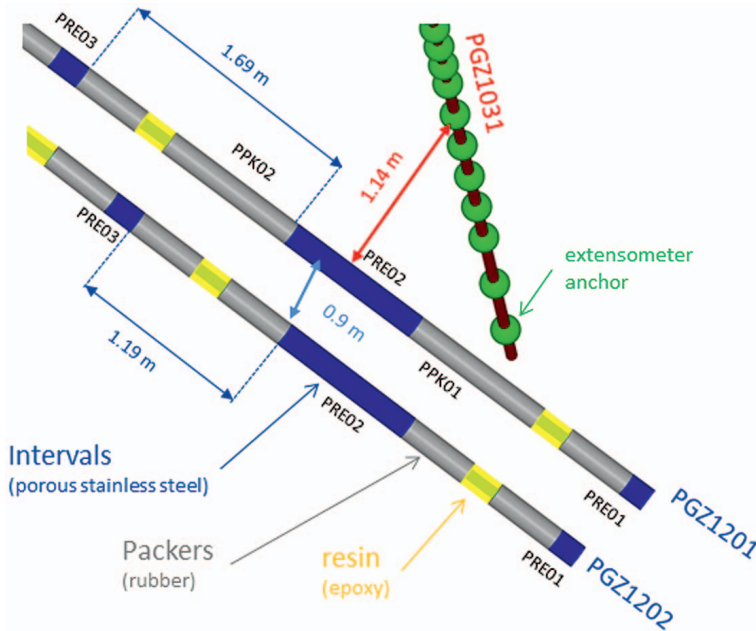


FIG. 10. Set up of the PGZ1 experiment showing the location and names of the test array.

GAS FLOW IN CALLOVO-OXFORDIAN CLAYSTONE

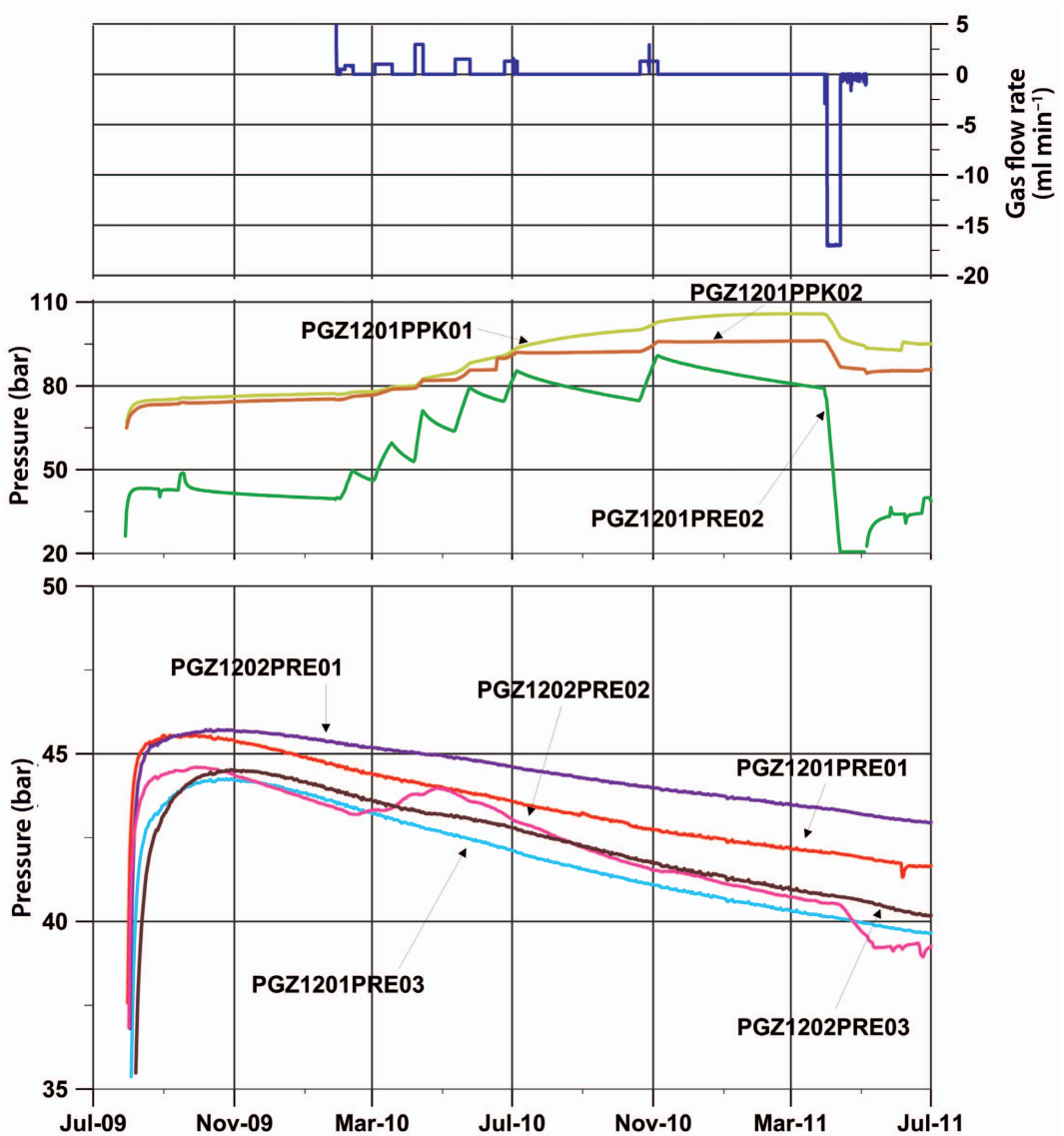


FIG. 11. Data from boreholes PGZ1201 and PGZ1202 showing the evolution of gas inflow as well as packer (PPK01 and PPK02 in borehole PGZ1201), gas and porewater pressures.

(Baechler *et al.*, 2011). Hydraulic conductivity values are 2.6×10^{-13} and $6.4 \times 10^{-11} \text{ m s}^{-1}$ for the external and internal zones, respectively. The discontinuity radius (equivalent to the damaged zone around the borehole) between the internal and external zones is assumed to be very close to the borehole wall (i.e. 4 cm). The hydraulic conductivity value for the external zone is

consistent with radial permeability values for intact rock derived from laboratory tests (hydraulic properties), suggesting flow may have been focussed along the bedding planes. At the end of January 2010, the synthetic fluid in PRE02 was replaced by nitrogen gas (at an equivalent pressure) and test GAS1 started on 1 February 2010 (Fig. 11).

Inspection of the data from Fig. 11 clearly shows an ‘interference’ observed in borehole PGZ1202 (interval PRE02), which is located about 90 cm from the gas injection interval. Conversely, no perturbation was observed in either signal from the piezometers located above (PRE03) and below (PRE01) the gas injection interval in borehole PGZ1201. These observations indicate that the injected gas gradually penetrates into the rock but does not pass along the borehole wall via the interface between the piezometer and the clay.

The response of interval PGZ1202_PRE02 is markedly different after the first three gas injection steps, showing a reduction in amplitude as pressure decays within the monitoring filter. In addition neither of the packers PPK01 or PPK02 (either side of the injection interval) show any kind of sensitivity to the reduction in gas pressure during the recovery period of each test stage.

Interpretation

Although every effort was made to remove the synthetic porewater prior to gas testing, residual water remained trapped within the filter volume of PGZ1201_PRE02. As such, it is likely this fluid will be preferentially mobilized before gas begins to penetrate the claystone.

Although the exact amount of residual water is unknown, it is possible to estimate its volume during the initial gas injection steps using the ideal gas law. Figure 12 depicts the pressure variation for each injection step compared to that calculated from the ideal gas law for different volumes of gas. The volume of gas equal to 804 cm³ corresponds to the pore volume of the filter, assuming full convergence around the test interval. In contrast, the volume of gas equal to 1540 cm³ assumes zero convergence with no creep of the borehole wall. Analysis of the data suggests the volume is close to this latter value

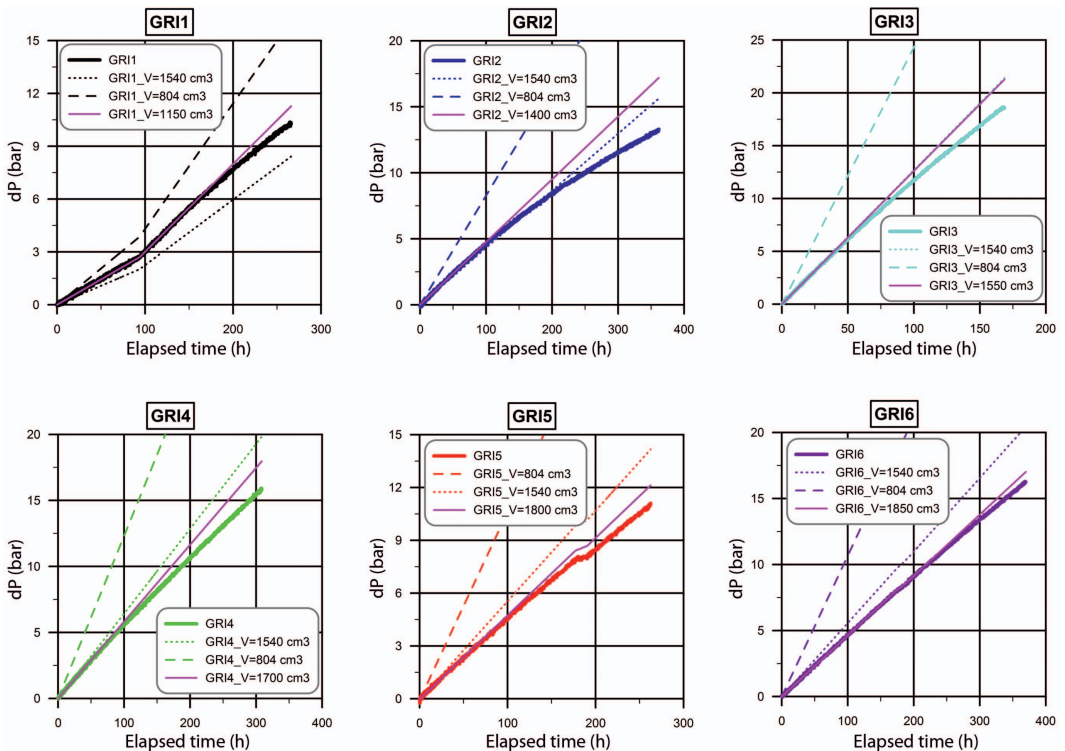


FIG. 12. Comparison of the pressure differential measured (bold line) and that calculated at constant volume with the ideal gas law for the six injection steps (GRI1 to GRI6). Large dashed line equal to minimum interval volume, dot line equal to maximum interval volume. The pink line is the best fit volume.

suggesting little convergence has occurred around the filter.

At the start of gas injection (GRI1), the estimated gas volume is close to 1150 cm³. During the next two steps (GRI2 and GRI3), the gas volume appears to increase but is still below the maximal volume calculated for PGZ1201_PRE02. However, between (GRI4 to GRI6), the gas volume is consistently higher than the maximal volume of the test array. This suggests that after GRI3, there is little, if any, residual water remaining in the test filter and gas has begun to locally penetrate the claystone. As such, the gas entry pressure is estimated to be around 2 MPa which corresponds to an average pore radius of 0.07 µm. This value is also close to that estimated from test COx-1 and corresponds to a pore radius more representative of disturbed claystone pore size.

After GRI3, the gas starts to percolate into the borehole damaged zone and moves preferentially around the bottom packer, caused by the drainage effect of borehole PGZ1031 which crosses PGZ1201 just above the bottom packer PPK01. Numerical modelling will be undertaken in the future to help interpret the data and identify if/when gas penetrates the intact host rock.

Conclusion

A series of long-term laboratory tests have been undertaken at the BGS to examine the fundamental mechanisms governing the migration of gas through COx. These measurements demonstrate the movement of gas is accompanied by dilation of the clay fabric (Angeli *et al.*, 2009). Under these conditions, gas flow is not within the original porosity of the clay but primarily along pressure-induced preferential pathways, similar in form to those suggested by Harrington and Horseman (1999). Here, permeability is a dependent variable related to the number, width and aperture distributions of these features. There is now a substantial body of evidence indicating gas pathways exhibit highly coupled dynamic behaviour, are inherently unstable and evolve spatially and temporally during tests. This hypothesis is further supported by post-test measurements of water saturation which indicate no discernible displacement of water from the COx, even when subject to large gas pressure gradients for extended periods of time. Early results from field scale tests suggest gas flow is primarily within the disturbed zone around the

piezometer interval and future tests will be performed to verify this result.

Acknowledgements

Funding for the study was provided by Andra (within the auspices of the “Transfert de Gaz” initiative), the European Atomic Energy Community’s Seventh Framework Programme (FP7/2007-2011) under Grant Agreement no. 230357, and the BGS through its well founded laboratory programme and the Geosphere Containment project (part of the BGS core strategic programme).

References

- Andra (2005) *Argile: Référentiel du site de Meuse/ Haute-Marne, Tome 2: Caractérisation Comportementale du Milieu Géologique sous Perturbation*. Andra, Chatenay-Malabry, France.
- Angeli, M., Soldal, M., Skurtveit, E. and Aker, E. (2009) Experimental percolation of supercritical CO₂ through a caprock. *Energy Procedia*, **1**, 3351–3358.
- Baechler, S., Lavanchy, J.M., Armand, G. and Cruchaudet, M. (2011) Characterisation of the hydraulic properties within the EDZ around drifts at level 490 mof the Meuse/ Haute-Marne URL: a methodology for consistent interpretation of hydraulic tests. *Physics and Chemistry of the Earth, Parts A/ B/C*, **36**, 1922–1931.
- de la Vaissière, R. and Talandier, J. (2012) *Gas Entry Pressure in Callovo-Oxfordian Claystone: in situ Experiment PGZ1*. Actes du Colloque National Transfert 2012/workshop organised in the framework of the EU FP7 project FORGE, Ecole Centrale de Lille/LML, 20–22 March 2012.
- de Marsily, G. (1986) *Quantitative Hydrogeology for Engineers*. Academic Press, Orlando, Florida, USA.
- Harrington, J.F. and Horseman, S.T. (1999) Gas transport properties of clays and mudrocks. Pp. 107–124 in: *Muds and Mudstones: Physical and Fluid Flow Properties* (A.C. Aplin, A.J. Fleet, and J.H.S. Macquaker, editors). Geological Society of London Special Publication, **158**. Geological Society of London, London.
- Harrington, J.F., Noy, D.J., Horseman, S.T., Birchall, J.D. and Chadwick, R.A. (2009) Laboratory study of gas and water flow in the Nordland Shale, Sleipner, North Sea. Pp. 521–543 in: *Carbon Dioxide Sequestration in Geological Media – State of the Science* (M. Grobe, J.C. Pashin and R.L. Dodge, editors) AAPG Studies in Geology, **59**. American Association of Petroleum Geologists, Tulsa, Oklahoma, USA

- Horseman, S.T., Harrington, J.F. and Sellin, P. (1996) Gas migration in Mx80 buffer bentonite. *Materials Research Society*, **465**, 1003–1010.
- Horseman, S.T., Harrington, J.F. and Sellin, P. (2004) Water and gas flow in Mx80 bentonite buffer clay. *Materials Research Society*, **807**, 715–720.
- Huyakorn, P.S. and Pinder, G.F. (1983) *Computational Methods in Subsurface Flow*. Academic Press, Orlando, Florida, USA.
- INTERA (1983) *STAFAN: A Two-Dimensional Code for Fluid Flow and the Interaction of Fluid Pressure and Stress in Fractured Rock for Repository Performance Assessment*. Office of Nuclear Waste Isolation Report ONWI 427.
- Ortiz, L., Volckaert, G. and Mallants, D. (2002) Gas generation and migration in Boom Clay, a potential host rock formation for nuclear waste storage. *Engineering Geology*, **64**, 287–296.
- Weetjens, E. and Sillen, X. (2006) *Gas Generation and Migration in the Near Field of a Supercontainer-Based Disposal System for Vitrified High-Level Radioactive Waste*. Proceedings of the 11th International High-Level Radioactive Waste Management Conf. (IHLRWM), Las Vegas, Nevada, USA.
- Wikramaratna, R.S., Goodfield, M., Rodwell, W.R., Nash, P.J. and Agg, P.J. (1993) *A Preliminary Assessment of Gas Migration from the Copper/Steel Canister*. SKB Technical report TR93-31.
- Wileveau, Y. and Bernier, F. (2008) Similarities in the hydromechanical response of Callovo-Oxfordian clay and Boom Clay during gallery excavation. *Physics and Chemistry of the Earth*, **33**, S343–S349.
- Zweigel, P., Moen, A. Vassenden, F. and Erdmann, M. (2006) *The role of hysteretic two-phase flow processes during capillary leakage*. American Association of Petroleum Geologists International Conference and Exhibition, Perth, 5–8 November 2006, [conference abstract].